Quantum dot attached to superconducting leads: Relation between symmetric and asymmetric coupling

A. Kadlecová, M. Žonda, and T. Novotný*

Department of Condensed Matter Physics, Faculty of Mathematics and Physics, Charles University, Ke Karlovu 5, CZ-121 16 Praha 2, Czech Republic

(Received 21 October 2016; revised manuscript received 13 January 2017; published 8 May 2017)

We study the Anderson single-level quantum dot attached to two BCS superconducting leads with the same gap size. We reveal that a system with asymmetric tunnel coupling to the leads ($\Gamma_L \neq \Gamma_R$) can be related to the symmetric system with the same net coupling strength $\Gamma = \Gamma_L + \Gamma_R$. Surprisingly, it is the symmetric case which is the most general, meaning that all physical quantities in the case of asymmetric coupling are fully determined by the symmetric ones. We give ready-to-use conversion formulas for the 0-π phase transition boundary, on-dot quantities, and the Josephson current and illustrate them on the NRG results of Oguri, Tanaka and Bauer [Phys. Rev. B **87**, 075432 (2013)] for the three-terminal setup. We apply our theory to the recent 0-π transition measurement of Delagrange *et al.* [Phys. Rev. B **93**, 195437 (2016)] and determine the asymmetry of the experimental setup from the measured transition width. Finally, we establish that the widely assumed Kondo "universality" of physical quantities depending only on the ratio of the Kondo temperature and the superconducting gap T_K/Δ cannot hold for asymmetric junctions.

DOI: 10.1103/PhysRevB.95.195114

I. INTRODUCTION

Superconducting quantum dot nanostructures generalizing the conventional Josephson junctions have been the subject of intensive research in the past decade [1,2]. Versatility of the setup covering a wide range of gate-tunable nanostructures [3–26] promises great potential for applications but also allows for detailed studies of their nontrivial physical properties including Josephson supercurrent and Andreev subgap transport. In many cases the system can be very well described by a simple single impurity Anderson model (SIAM) coupled to BCS leads [27] which, depending on particular parameters, may exhibit so-called 0-π transition signaled by the sign reversal of the supercurrent [7,9,10,16,20,24,25] and crossing of Andreev bound states (ABS) at the Fermi energy [18,22,28]. The 0-π transition is induced by the underlying impurity quantum phase transition (QPT) related to the crossing of the lowest many-body eigenstates of the system from a spin-singlet ground state with positive supercurrent (0 phase) to a spin-doublet state with negative supercurrent (π phase) [27,29–38].

In this study, we address an aspect of the problem which has been largely overlooked thus far, namely the systematic study of effects of asymmetry of the coupling to the two superconducting leads. Asymmetric coupling is quite generic in experiments, while theory typically addresses the symmetric setup for simplicity (and lack of resources to cover many asymmetric instances). In the normal nonequilibrium transport, the symmetric setup is indeed just a special case in the continuum of possibilities covering all asymmetries (while keeping the total coupling constant). However, as we show here, for the superconducting SIAM the symmetric case is the most general and all quantities for asymmetric situations can be derived *exactly* from it by simple analytical prescriptions. Despite their simplicity, their nontrivial implications concern both the fundamental properties of the model and the analysis of experiments.

*tno@karlov.mff.cuni.cz

II. SYMMETRIC-ASYMMETRIC RELATION

A. Theory

The single impurity Anderson model is described by the Hamiltonian

$$\mathcal{H} = \mathcal{H}_{\rm dot} + \sum_{\alpha} \left(\mathcal{H}^{\alpha}_{\rm lead} + \mathcal{H}^{\alpha}_{T}\right), \tag{1a}$$

where $\alpha = L, R$ denotes the left and right superconducting leads (and possibly additional normal-metal leads like in Refs. [39–42]). The first term

$$\mathcal{H}_{\rm dot} = \epsilon \sum_{\sigma=\uparrow,\downarrow} d^{\dagger}_{\sigma} d_{\sigma} + U d^{\dagger}_{\uparrow} d_{\uparrow} d^{\dagger}_{\downarrow} d_{\downarrow} \tag{1b}$$

describes an impurity with a single-particle level ϵ. Operators $d^{\dagger}_{\sigma}, d_{\sigma}$ create (annihilate) an on-dot electron with spin σ, and U describes the local Coulomb interaction. The BCS Hamiltonian of the superconducting leads reads

$$\mathcal{H}^{\alpha}_{\rm lead} = \sum_{\mathbf{k}\sigma} \epsilon_{\alpha}(\mathbf{k})\, c^{\dagger}_{\alpha\mathbf{k}\sigma} c_{\alpha\mathbf{k}\sigma} - \Delta_{\alpha} \sum_{\mathbf{k}} (e^{i\varphi_{\alpha}} c^{\dagger}_{\alpha\mathbf{k}\uparrow} c^{\dagger}_{\alpha\,-\mathbf{k}\downarrow} + \text{H.c.}), \tag{1c}$$

where $c^{\dagger}_{\alpha\mathbf{k}\sigma}, c_{\alpha\mathbf{k}\sigma}$ are the creation and annihilation operators of electrons with momentum $\mathbf{k}$ and spin σ, Δ_{α} is the amplitude of the superconducting gap, and φ_{α} is the superconducting phase. Throughout this paper we will assume $\Delta_L = \Delta_R = \Delta$, which is crucial for our derivation (and generic in experiments). The last term

$$\mathcal{H}^{\alpha}_{T} = \sum_{\mathbf{k}\sigma} (t_{\alpha\mathbf{k}} c^{\dagger}_{\alpha\mathbf{k}\sigma} d_{\sigma} + \text{H.c.}) \tag{1d}$$

describes the coupling with t_{α} denoting the tunneling matrix elements. We assume the tunnel-coupling magnitude $\Gamma_{\alpha} = \pi t^2_{\alpha} \rho_{\alpha}$ (where ρ_{α} is the normal-state density of lead electron states at the Fermi level) to be constant in the energy range of interest. We further denote $\Gamma \equiv \Gamma_R + \Gamma_L$.

The system can be described in the Matsubara formalism [43–45]. In the noninteracting $U = 0$ case the Green function reads

$$\widehat{G}_0(i\omega_n)=\begin{pmatrix} i\omega_n[1+s(i\omega_n)]-\epsilon & \Delta_\varphi(i\omega_n) \\ \Delta^*_\varphi(i\omega_n) & i\omega_n[1+s(i\omega_n)]+\epsilon \end{pmatrix}^{-1}, \tag{2}$$

where ω_n are fermionic Matsubara frequencies and the functions $s(i\omega_n) = \Gamma/\sqrt{\omega_n^2+\Delta^2}$ and $\Delta_\varphi(i\omega_n) = (\Gamma_L e^{i\varphi_L} + \Gamma_R e^{i\varphi_R})\Delta/\sqrt{\omega_n^2+\Delta^2}$.

The interacting ($U \neq 0$) system with self energy Σ is then described by the full Green function $\widehat{G}$, which is given by the Dyson equation $\widehat{G}^{-1}(i\omega_n) = \widehat{G}_0^{-1}(i\omega_n) - \widehat{\Sigma}(i\omega_n)$. The Green function $\widehat{G}$ is known to be a functional of $\widehat{G}_0$, only further depending on the interaction strength U [43], meaning that model parameters Γ_α, φ_α, ϵ only enter through $\widehat{G}_0$. Any symmetries of the noninteracting system under the change of these parameters are then preserved in the interacting case. We will further deal with a correspondence of the case of symmetric coupling ($\Gamma_L = \Gamma_R = \Gamma/2$) with an asymmetric case ($\Gamma_L \neq \Gamma_R$), accompanied by a corresponding change in the φ_α parameters.

We first notice that $\widehat{G}_0$ only depends on $\varphi_{L,R}$ through the off-diagonal part Δ_φ and, moreover, only through a frequency-independent factor $\Gamma_L e^{i\varphi_L} + \Gamma_R e^{i\varphi_R}$. Introducing the superconducting phase difference $\varphi = \varphi_L - \varphi_R$, $\varphi \in (-\pi,\pi)$, the average phase shift $\delta = (\varphi_L + \varphi_R)/2$, and the coupling-parameter asymmetry $a \equiv \Gamma_L/\Gamma_R$, we can now simplify the φ-dependent factor to

$$\Gamma_L e^{i\varphi_L} + \Gamma_R e^{i\varphi_R} = \Gamma\sqrt{\chi(\varphi,a)}e^{i(\delta+\Psi)}, \tag{3a}$$

with

$$\chi(\varphi,a) = 1 - \frac{4a}{(a+1)^2}\sin^2\frac{\varphi}{2} \tag{3b}$$

and the overall phase Ψ

$$\Psi(\varphi,a) = \arctan\left[\left(\frac{a-1}{a+1}\right)\tan\frac{\varphi}{2}\right]. \tag{3c}$$

Equations (3a)–(3c) make it possible to relate an asymmetric junction to a symmetric one. Note that $\chi(\varphi,a)$ is preserved by $a \to 1/a$ (thus reflecting our freedom of choice in the definition of the asymmetry) and reduces to $\chi(\varphi,1) \equiv \cos^2(\varphi/2)$ in the symmetric case. The value range of $\chi(\varphi,a=1)$ in the symmetric case is $[0,1]$, which shrinks to $[(a-1)^2/(a+1)^2,1]$ for the asymmetric one ($a \neq 1$). Together with continuity and monotony of function $\chi(\varphi)$ this implies that for any physical (asymmetric) φ^A there exist an effective (symmetric) φ^S such that

$$\chi(\varphi^S,1) = \chi(\varphi^A,a). \tag{4}$$

Inserting from Eq. (3b) we find that

$$\varphi^S = 2\arccos\sqrt{\chi} = 2\arccos\sqrt{1 - \frac{4a}{(a+1)^2}\sin^2\frac{\varphi^A}{2}}. \tag{5a}$$

To express φ^A instead, we invert this formula and using (3b) together with $2\arcsin x = \arccos(1-2x^2)$ we obtain

$$\begin{aligned}\varphi^A &= \arccos\left(\frac{(a+1)^2}{2a}(\chi-1)+1\right) \\ &= \arccos\left(1 - \frac{(a+1)^2}{2a}\sin^2\frac{\varphi^S}{2}\right).\end{aligned} \tag{5b}$$

Eqs. (5a) and (5b) are substitution relations for φ, which are sufficient to relate on-dot quantities. To ensure correspondence of nonlocal quantities such as the Josephson current, we also have to impose the condition

$$\delta^S = \delta^A + \Psi(\varphi^A), \tag{5c}$$

which ties together the gauges of the symmetric and asymmetric cases. Equations (5a) and (5c) fully describe the correspondence, ensuring $\widehat{G}(\varphi^A,\delta^A) = \widehat{G}(\varphi^S,\delta^S)$.

We wish to stress that counterintuitively it is the *symmetric* case which contains all information and only needs to be examined to fully understand the general (asymmetric) system. This is very useful, because it allows us to calculate only characteristics of the symmetric case and then compute all other cases from the formulas above. Additionally, it is also a simple way to determine the asymmetry of an experimental setup.

B. Phase boundary

We will now examine specific examples of the symmetric-asymmetric relation, starting with the 0-π *phase boundary*. In a suitable range of parameters, when keeping U, Γ, and Δ fixed, the state of the system depends on ϵ and φ and may exhibit the 0-π transition. The transition curve is described by $\varphi_C(\epsilon)$, φ_C being the critical value at which the transition occurs for a given ϵ. Knowing the relation $\varphi_C^S(\epsilon)$ in the symmetric case, we simply get the asymmetric transition curve by substitution in Eq. (5b). Figure 1 shows the phase diagram for different values of U, in symmetric and asymmetric cases. The parameters $\Gamma = 0.44$ meV, $\Delta = 0.17$ meV correspond to the experiment of Delagrange *et al.* [25] which will be addressed in more detail later on. The symmetric curves in panel (a) were obtained by numerical renormalization group (NRG) calculations [46]. For small enough U [2 and 2.5 meV in Fig. 1(a)] the π phase exists only above some finite critical φ_C^S even at $\epsilon = -U/2$. The φ_C^S curve changes to approximately arc-cosine shape for larger U. Part (b) shows the effect of asymmetry. The curves were obtained from panel (a) by using the relation (5b). Only the lower part of the symmetrical data in panel (a) is used and gets "stretched" by transformation (5b) over the whole φ range (consequently, the phase boundary line corresponding to $U = 2$ disappears altogether). Panel (c) shows a plot of $1 - \chi(\varphi_C)$ dependence on $\tilde{\epsilon} \equiv (\epsilon + U/2)/(U/2) = 1 + 2\epsilon/U$. Due to Eq. (4), χ can be with advantage used as an invariant variable.

C. Physical quantities

Physical quantities on the dot, like the free energy, particle number, magnitude of the induced gap, or energy of the Andreev bound states, which depend only on the local Green function in a gauge-invariant way (i.e., are independent of δ), can

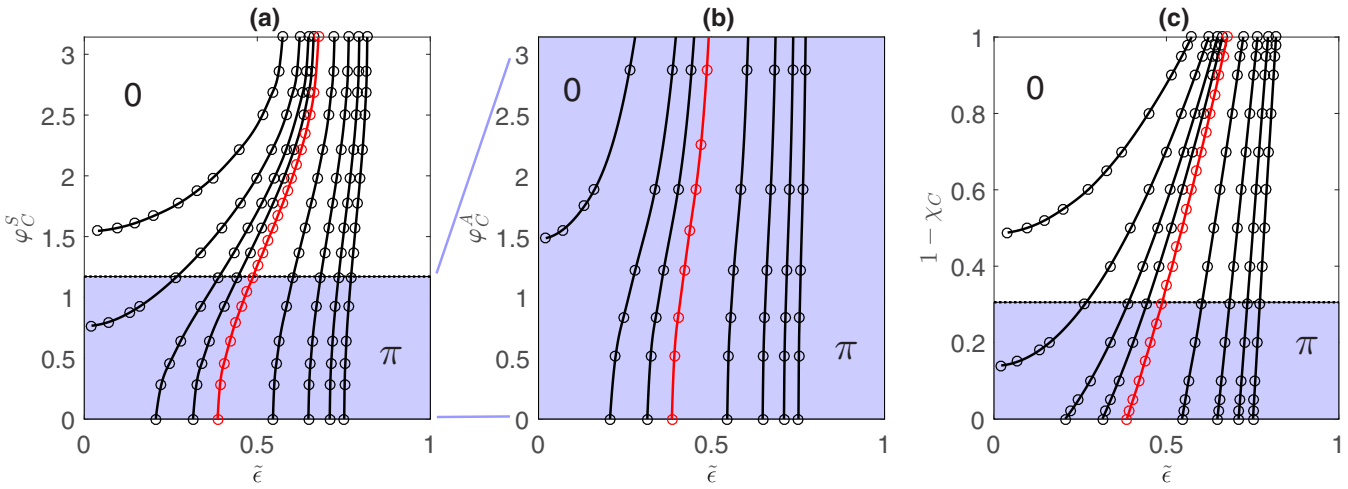

FIG. 1. 0-π phase boundary. (a) φ_C^S dependence on the (shifted and normalized) energy level $\tilde{\epsilon} \equiv 1 + 2\epsilon/U$ in the symmetric case $\Gamma_L = \Gamma_R$. The dots were obtained by NRG using the parameters $\Gamma = 0.44$ meV, $\Delta = 0.17$ meV, and (from left to right) $U = \{2, 2.5, 2.8, 3, 3.2, 4, 5, 6, 7\}$ meV. The red line ($U = 3.2$ meV) represents the experimental values of Delagrange *et al.* [25]. (b) $\varphi_C^A(\epsilon)$—plot (a) recomputed via Eq. (5b) for asymmetry $a = 11$. The relevant φ_C^S range is indicated by the blue area in panels (a) and (c). (c) $1 - \chi(\varphi_C)$ vs the shifted and normalized dot level energy ϵ. The curves are becoming linear with increasing U.

also be computed easily. If the quantity's φ dependence $F^S(\varphi^S)$ is known in the symmetric case, the symmetric-asymmetric relation reads $F^A(\varphi^A) = F^S(\varphi^S)$. Inserting Eq. (5a) yields for any asymmetry a the equation

$$F(\varphi) = F^S\left(2\arccos\sqrt{1 - \frac{4a}{(a+1)^2}\sin^2\frac{\varphi}{2}}\right). \tag{6}$$

Here, $F(\varphi)$ and φ are the physical quantities that can be measured/tuned experimentally in a real asymmetric junction (we skip the superscript A for physical quantities from now on).

If we want to describe the *Josephson current*, which is represented by a nonlocal operator coupling the dot to lead(s), we encounter a problem as its mean value is not determined from the Green's function $\widehat{G}$ only but depends explicitly on φ_α as well [45]. If one proceeds via this direct way, relation (5c) must be also incorporated into the (rather tedious) derivation as we explicitly demonstrate in Appendix A. However, it is possible to follow an indirect route of the supercurrent evaluation via the derivative $J \equiv 2e/\hbar \cdot \partial F/\partial\varphi$ of the free energy F, which satisfies the above symmetry relation (6). Consequently, a prefactor appears in the symmetric-asymmetric relation for the supercurrent:

$$J(\varphi) = \frac{\cos\frac{\varphi}{2}}{\sqrt{\frac{(a+1)^2}{4a} - \sin^2\frac{\varphi}{2}}} \times J^S\left(2\arccos\sqrt{1 - \frac{4a}{(a+1)^2}\sin^2\frac{\varphi}{2}}\right). \tag{7}$$

Note that our theory can also be used if the setup contains one or more normal metal lead(s) in addition to the two superconductors like in Refs. [39–42], because the normal metal leads do not influence the physics of the superconducting phase difference. This is illustrated in Fig. 2 containing different on-dot quantities and the Josephson current for a setup with an additional normal electrode. The black bullets were taken graphically from Fig. 11 of Ref. [40], where they were calculated by NRG for symmetric as well as asymmetric cases. On the other hand, we calculated by NRG only the blue lines for the symmetric case, while red lines, corresponding to different levels of asymmetry, were obtained by Eq. (6) for on-dot quantities and Eq. (7) for the Josephson current. With higher asymmetry, a smaller range of the symmetric data is used. The on-dot quantities (a)–(c) are characteristically "stretched," while the behavior of the Josephson current (d) is more complicated due to the prefactor in Eq. (7). In particular

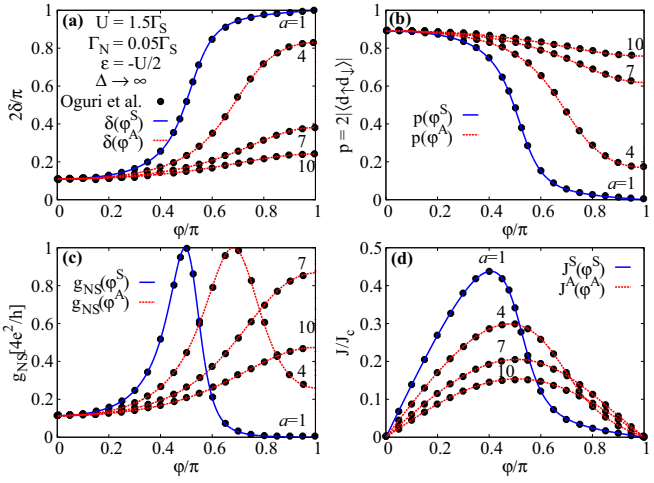

FIG. 2. Phase shift δ (a), magnitude of the pair correlation (b), Andreev conductance g_{NS} (c), and Josephson current J in terms of $J_C = e\Gamma_S/\hbar$ (d) plotted as functions of the Josephson phase difference φ. The black bullets have been taken graphically from Fig. 11 in Oguri *et al.* [40]. The blue solid lines have been calculated for the symmetric coupling ($a = 1$) using the NRG. The red dashed lines, representing asymmetric coupling with $a = 4, 7, 10$ have been obtained from the blue ones using the relations (6) (a)–(c) and (7) (d).

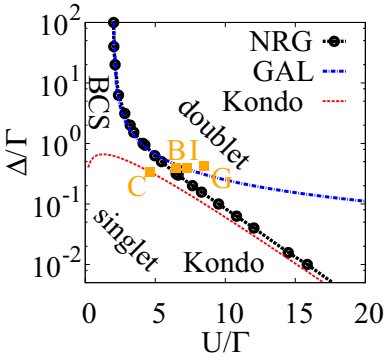

FIG. 3. Phase diagram in the U-Δ plane of the superconducting single-impurity Anderson model with symmetric leads at half-filling $\epsilon = -U/2$ and $\varphi = 0$ (note the logarithmic scale on the vertical axis). Black line separates the singlet (0 phase) and doublet (π phase) ground states. The 0 phase has two kinds of singlet ground state (BCS and Kondo) connected through a broad crossover region. NRG solution (black bullets) is compared with the GAL approximation [44,45] (blue dash-dotted line) and with an estimate of the critical delta from the Kondo temperature $\Delta_C \approx 1.37\,T_K$ [32] (red dashed line). The orange squares mark the positions of the experimental setup taken from Ref. [25].

$J(\varphi = \pi) = 0$ also for the asymmetric cases. Our theory is in all cases in excellent agreement with NRG results.

D. Kondo (non)universality

We wish to comment on the notion of Kondo universality used, e.g., in Ref. [25]. If the system is in the Kondo regime (big U/Γ and small enough Δ/Γ, see Fig. 3), physical quantities are believed to only depend on T_K/Δ, where

$$T_K = \sqrt{\frac{\Gamma U}{2}} \exp\left(-\frac{\pi\left|4\epsilon^2 - U^2\right|}{8\Gamma U}\right) \tag{8}$$

is the normal-state Kondo temperature. To our knowledge, in the superconducting case universality has been tested both by numerical simulations of a symmetric setting [32–34] and experimentally [47]. As our example of the transition width demonstrates, physical quantities can be altered by the asymmetry of the junction while keeping Γ and, thus, also T_K constant—recall the disappearance of the transition line corresponding to $U = 2$ meV ($U/\Gamma \approx 4.5$) between panels (a) and (b) of Fig. 1. Consequently, T_K/Δ scaling cannot hold for junctions with different asymmetry and there is at least one more parameter to be taken into account for any physical quantity F: $F^S(T_K/\Delta) \longrightarrow F(T_K/\Delta, a)$.

III. ANALYSIS OF THE EXPERIMENT

One of the most beneficial outcomes of the symmetric-asymmetric relation is that all relevant experiments can be addressed with the symmetric models regardless of the real coupling asymmetry. Moreover, Eq. (5b) can be used to obtain the value of the asymmetry from the experimental data as we now demonstrate.

In their recent experimental study of a carbon nanotube (CNT) quantum dot, Delagrange *et al.* [25] focused on the 0-π transition controlled by the superconducting phase difference φ. Parameters of the single impurity Anderson model pertinent to the sample have been extracted from typical Coulomb diamonds appearing in the stability diagram and are summarized in Table I. The authors have successfully fitted the 0-π phase transition curve $\varphi_C(\epsilon)$ on both sides of three Coulomb diamonds (called B, G, and I) with an arc-cosine dependence

$$\varphi_C = \arccos\left\{-2\frac{\epsilon - \epsilon_t}{\delta\epsilon}\right\} \tag{9}$$

linear in energy. Here, $\delta\epsilon$ is the full width and ϵ_t is the position of the center of the transition curve. This suggests an interesting universality, which, however, was not followed by the diamond C where formula (9) had to be replaced by $\varphi_C \sim \arccos(c + \tilde{\epsilon}^2)$ [25]. This was reportedly because the transition took place close to $\tilde{\epsilon} = 0$ and because it was "incomplete," i.e., observed only above some finite critical φ_C as in our Fig. 1.

It should be mentioned that the arc-cosine functional form is necessary from the upper of Eq. (5b); it is the *energy dependence* (linear or quadratic) which is nontrivial. To understand the energy-dependence behavior we first plot in Fig. 3 a generic phase diagram in the $\Delta/\Gamma - U/\Gamma$ plane for $\varphi = 0$, symmetric coupling to the leads, and at half-filling ($\epsilon = -U/2$; $\tilde{\epsilon} = 0$). There are three regions: π phase where the ground state is a spin doublet and 0 phase with the BCS and Kondo singlet ground state regions [44,45]. As can be seen the phase boundary calculated via NRG (black bullets) approaches in the Kondo region (small Δ) the analytical curve [48] $\Delta_C \approx 1.37\,T_K$ (red line in Fig. 3), which was discussed in detail in Ref. [32]. On the other hand, we recently showed [44,45] that the phase boundary in the BCS region and close to the half-filling can be very well approximated by a simple generalized atomic limit (GAL) formula $\chi_C =$

TABLE I. Transition width and asymmetry—summary of experimental data [25] and our corresponding results. Columns correspond to the measured Coulomb diamonds. The rows give the measured normalized parameters U/Γ, Δ/Γ, and coefficients α and γ of Eq. (10) obtained from the NRG data fitting. Normalized transition widths $\widetilde{\delta\epsilon}_{\rm exp} \equiv 2\delta\epsilon_{\rm exp}/U$ measured for both sides of the diamonds are followed by the asymmetry a determined by the procedure discussed in the main text. The last two lines are parameters (negative slope and asymmetry) obtained by an alternative linearization fitting procedure, which is discussed in Appendix B. (#) Here, $\widetilde{\delta\epsilon}_{\rm exp}$ is bigger then the transition width of the symmetric case (see the main text for details).

	B		C		G		I	
	left	right	left	right	left	right	left	right
U/Γ	6.5		4.6		8.5		7.3	
Δ/Γ	0.4		0.34		0.425		0.39	
α	2.82		1.53		4.27		3.26	
γ	1.22		0.47		2.21		1.50	
$\widetilde{\delta\epsilon}_{\rm exp}$	0.23	0.43	0.87	0.96	0.06	0.06	0.15	0.2
$\boldsymbol{a}$	**5.7**	**1#**	**1#**	**1#**	**11.8**	**11.8**	**6.6**	**4.0**
$\beta^A_{\rm NRG}$	0.479	#			0.202	0.202	0.347	0.317
$a_{\rm lin}$	5.8	1#			11.4	11.4	6.4	4.0

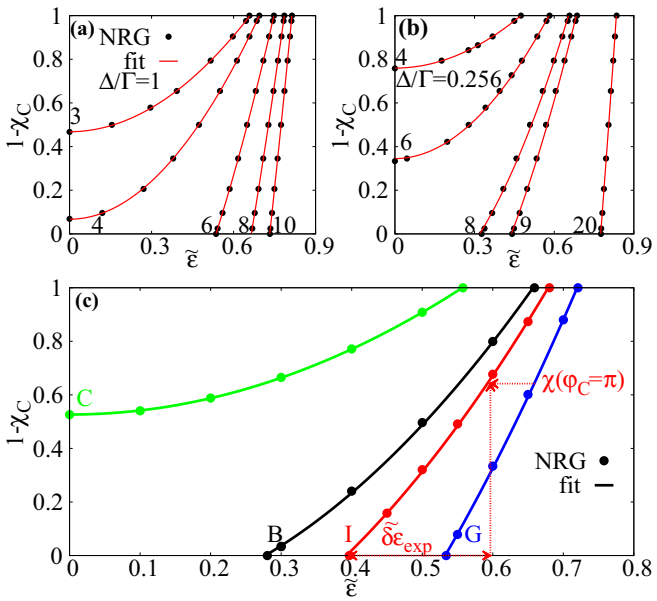

FIG. 4. Dependence of critical χ_C on $\tilde{\epsilon}$ calculated using NRG (dots) and fitted by the parabola Eq. (10). (a) For $\Delta/\Gamma = 1$ the least-square fit error stayed below 0.2% for all plotted values of U/Γ (indicated by the numbers next to the curves). (b) Case $\Delta/\Gamma = 0.256$ had the biggest least-square fit error from all discussed cases; however, it was still below 1.2% for all plotted values of U/Γ. (c) Curves for all diamonds from Table I. As an example we marked the point $\chi(\varphi_C = \pi)$ used in Eqs. (12) and (13) for the right side of the diamond I. Its position was obtained using the measured value of $\widetilde{\delta\epsilon}_{\rm exp}$.

$(U/2\Gamma)^2[1/(1+\Gamma/\Delta)^2 - \tilde{\epsilon}^2]$ shown as the blue line in Fig. 3 (with $\chi_C = 1$ and $\tilde{\epsilon} = 0$). We also depict as orange squares the experimental values of the Δ and U parameters normalized by total Γ for diamonds B, C, G, and I discussed here (notice that their placement in the phase diagram is only approximate as the phase transitions in those diamonds do not happen at the assumed half-filling).

Interestingly, all the considered diamonds lie in the intermediate region where neither of the above two analytical formulas work (see the orange squares in Fig. 3). Nevertheless, we have discovered by exhaustive analysis of the NRG data that in compliance with GAL the critical $\chi_C(\tilde{\epsilon})$ can be for sufficiently high Δ/Γ nearly perfectly fitted with a parabola

$$\chi_C(\tilde{\epsilon}) = \gamma - \alpha\tilde{\epsilon}^2, \tag{10}$$

although the coefficients α and γ differ from the GAL values. The examples of fits for different Δ/Γ and U/Γ are shown in Fig. 4. We have found out that the least-square-fitting errors [49] are below 0.5% for both $\Delta/\Gamma = 1$ [panel (a)] as well as for $\Delta/\Gamma \sim 0.3$ [panel (c) corresponding to the experimental data from Fig. 3]. Even for the lowest considered ratio $\Delta/\Gamma = 0.256$ (motivated by diamond A in Ref. [25] not further discussed in here) was the difference from a parabola below 1.2%. However, the parabolic dependence breaks down for still smaller values of Δ/Γ (we have observed its clear breakdown already for $\Delta/\Gamma = 0.1$; not shown) and it is definitely not valid in the strong Kondo regime. Yet, the above tests show that Eq. (10) can be safely used for analysis of all considered diamonds.

This simple observation explains both above experimental findings. After inserting Eq. (10) into Eq. (5b), which leads to

$$\varphi_C = \arccos\left[\frac{(a+1)^2}{2a}\left(\gamma - \alpha\tilde{\epsilon}^2 - \frac{a^2+1}{(a+1)^2}\right)\right], \tag{11}$$

one can immediately see that the seemingly anomalous transition for the diamond C with the quadratic energy dependence [see Fig. 4(c)] is actually quite generic. On the other hand, the allegedly universal linear energy dependence of χ_C shown in Fig. 1(c) and Fig. 4 is in fact a limit of parabolas with large coefficients α.

Parabolic character of the phase transition curve can be used to easily obtain the asymmetry of the experimental setups either by fitting the experimental data with Eq. (11) or just by using a simple formula obtained from Eq. (3b) (with the chosen solution $a > 1$)

$$a = \frac{1+\sqrt{\chi(\varphi_C = \pi)}}{1-\sqrt{\chi(\varphi_C = \pi)}}, \tag{12}$$

where $\chi(\varphi_C = \pi)$ can be read off from the theoretical curves using the normalized width of the transition $\widetilde{\delta\epsilon}_{\rm exp} \equiv 2\delta\epsilon_{\rm exp}/U$ measured in the experiment as illustrated in Fig. 4(c). Alternatively, for complete transitions when φ_C covers the whole 0 to π range [corresponding to large enough U cases in Figs. 1 and 4; B, G, and I diamonds in the experiment, see Fig. 4(c)] one can directly calculate $\chi_C(\varphi_C = \pi)$ from Eq. (10) as

$$\chi(\varphi_C = \pi) = 1 - 2\sqrt{\alpha(\gamma-1)}\widetilde{\delta\epsilon}_{\rm exp} - \alpha\widetilde{\delta\epsilon}^2_{\rm exp}. \tag{13}$$

The big advantage of determining the asymmetry a from formulas (12) and (13) is that the transition width $\delta\epsilon$ is a robust quantity [25,45] and that coefficients α and γ can be easily extracted from a few points (actually in the ideal case from just two) of the phase boundary calculated for the symmetrical coupling using, e.g., NRG [50].

In their experiment, Delagrange *et al.* [25] have determined the transition widths on both sides of the diamonds B, C, G, and I. For the right side of diamond I the asymmetry $a = 4$ was found via quantum Monte Carlo (QMC) simulations [24]; for B, C, G, and the left side of I it remained unknown. We have applied Eq. (12) to find the asymmetry of each diamond from the measured $\widetilde{\delta\epsilon}_{\rm exp}$ and coefficients γ and α obtained by fitting the symmetric-coupling phase boundaries $\chi_C(\epsilon)$ calculated via NRG shown in Fig. 4(c) (dots) with formula (10) (solid lines). The results are summarized in Table I. Analysis of the right side of diamond I [red lines in Figs. 1 and 4(c)] with the measured transition width $\widetilde{\delta\epsilon}_{\rm exp} = 0.20$ has given the asymmetry $a = 4$, which agrees with the value obtained earlier via QMC [24]. The values of a obtained for the diamond G and left sides of diamonds I and B point to even bigger asymmetries. On the other hand the normalized transition width $\widetilde{\delta\epsilon}_{\rm exp}$ measured on the right side of diamond B suggests a symmetric junction. The measured value ($\widetilde{\delta\epsilon}_{\rm exp} = 0.43$) is actually even wider than the width calculated for the symmetric coupling ($\widetilde{\delta\epsilon} = 0.39$), but the difference is within the 10% experimental uncertainty. For the diamonds B, I, and G, where the phase transition curves are close to linear, we also present the results ($a_{\rm lin}$) of an alternative fitting procedure based on linearization,

which was motivated by Eq. (9). This linearization procedure, which might be the only alternative in the strong Kondo regime, is discussed in detail in Appendix B. The asymmetries obtained by both methods are in good agreement.

Unfortunately, the analysis of the remaining diamond C is still problematic. Unlike in other diamonds, the phase transition for diamond C is incomplete, i.e., it only exists above some finite critical value of φ_C [Fig. 4(c)] as was also clearly observed in the experiment. The measured values ($\widetilde{\delta\epsilon}_{\rm exp} = 0.87$ and 0.96) are significantly bigger than the calculated width of the symmetric case ($\widetilde{\delta\epsilon} = 0.6$). One can perhaps assume that the large difference could happen as a combination of the 10% uncertainties in the estimation of the diamond's parameters and the error in the fitted transition width. In any case, the big value of $\widetilde{\delta\epsilon}_{\rm exp}$ hints at a symmetric or nearly symmetric junction.

IV. CONCLUSIONS

We have unveiled the thus far unnoticed simple, yet very powerful correspondence between the characteristics of a single-level quantum dot coupled symmetrically or asymmetrically to two phase-biased superconducting leads and potentially to further normal lead(s). We have found that, counterintuitively, the symmetric setup is the most general one and its knowledge allows full description of the equivalent asymmetric system for any value of the asymmetry of the coupling. This discovery makes it possible to utilize known results for symmetric setups in general asymmetric cases via trivial analytical relations. Moreover, it also provides an efficient tool for estimating the coupling asymmetry from the experimental data, which is otherwise a demanding task.

We have demonstrated the potential of this method by its application to recent experimental data in combination with a phenomenological analysis of the structure of phase-transition curves. We have discovered by exhaustive NRG calculations that the phase boundaries in a wide range of parameters (away from strong Kondo regime) are described by a simple quadratic functional dependence whose two parameters can be obtained with a moderate computational effort and utilized in a trivial analytical evaluation of the coupling asymmetry from the measured phase-transition width. In case of the single previously existing theoretical asymmetry prediction obtained by direct quantum Monte Carlo simulations for the given experiment, our result is in perfect agreement at a fractional computational cost.

ACKNOWLEDGMENTS

This work is supported by the National Science Centre (Poland) through the Grant No. DEC-2014/13/B/ST3/04451, the Czech Science Foundation via Project No. 16-19640S, and the Charles University Project GA UK No. 888217.

APPENDIX A: DERIVATION OF THE SYMMETRIC-ASYMMETRIC RELATION FOR THE JOSEPHSON CURRENT

The main aim of Appendix A is to show a direct derivation of the symmetric-asymmetric relation for the Josephson current. Not only should this serve as an illustration of the procedure but also as a guide for the derivation of other quantities which depend not only on the Green function but also explicitly on φ_α's.

Starting with the *interacting* Green function $\widehat{G}(i\omega_n)$, the Josephson current flowing into lead α can be expressed as a sum over Matsubara frequencies [45]

$$J_\alpha = 4k_BT\sum_{\omega_n}\frac{\Gamma_\alpha\Delta}{\sqrt{\Delta^2+\omega_n^2}}\mathrm{Im}[\mathcal{G}(i\omega_n)e^{-i\varphi_\alpha}], \tag{A1}$$

where T denotes the temperature and $\mathcal{G}(i\omega_n)$ is the off-diagonal element of $\widehat{G}(i\omega_n)$. As this expression explicitly depends on φ_α, we will have to handle the correspondence between the symmetric and asymmetric case as having two parameters, the phase difference $\varphi = \varphi_L - \varphi_R$ and shift $\delta = (\varphi_L + \varphi_R)/2$. As shown in the main text, these are connected by the transformation

$$\begin{aligned}\varphi^S &= 2\arccos\sqrt{\chi(\varphi^A)},\\ \delta^S &= \delta^A + \Psi(\varphi^A),\end{aligned} \tag{A2}$$

with $\chi(\varphi^A) = 1 - \frac{4a}{(a+1)^2}\sin^2\frac{\varphi^A}{2}$, and $\Psi(\varphi^A) = \arctan\left[\left(\frac{a-1}{a+1}\right)\tan\frac{\varphi^A}{2}\right]$, and asymmetry $a \equiv \Gamma_L/\Gamma_R$. We equivalently express the parameters φ_L^S, φ_R^S directly, obtaining

$$\begin{aligned}\varphi_L^S &= \tfrac{1}{2}\left(\varphi_L^A + \varphi_R^A\right) + \Psi(\varphi^A) + \arccos\sqrt{\chi(\varphi^A)},\\ \varphi_R^S &= \tfrac{1}{2}\left(\varphi_L^A + \varphi_R^A\right) + \Psi(\varphi^A) - \arccos\sqrt{\chi(\varphi^A)}.\end{aligned} \tag{A3}$$

With this choice of symmetric-asymmetric relation the Green function (and in particular it's off diagonal element) is preserved, so that $\mathcal{G}(\varphi_L^A,\varphi_R^A) \equiv \mathcal{G}(\varphi_L^S,\varphi_R^S)$. To compute the current we first denote

$$\begin{aligned}\mathcal{I} &= 2k_BT\sum_{\omega_n}\frac{\Gamma\Delta}{\sqrt{\Delta^2+\omega_n^2}}\mathrm{Im}[\mathcal{G}(i\omega_n)],\\ \mathcal{R} &= 2k_BT\sum_{\omega_n}\frac{\Gamma\Delta}{\sqrt{\Delta^2+\omega_n^2}}\mathrm{Re}[\mathcal{G}(i\omega_n)].\end{aligned} \tag{A4}$$

Then Eq. (A1) gives in the symmetric case

$$J_\alpha^S = \mathcal{I}\cos\varphi_\alpha^S - \mathcal{R}\sin\varphi_\alpha^S. \tag{A5}$$

Here we have used $\Gamma = 2\Gamma_\alpha$ and evaluated the imaginary part of $\mathcal{G}(i\omega_n)e^{-i\varphi_\alpha}$. From the current conservation law $J = J_L = -J_R$ and Eq. (A5) we get two equations ($\alpha = L,R$) for $\mathcal{I}$ and $\mathcal{R}$ with J as the parameter, leading to

$$\begin{aligned}\mathcal{I} &= -\frac{J^S}{\sin\varphi^S}\left(\sin\varphi_R^S + \sin\varphi_L^S\right),\\ \mathcal{R} &= -\frac{J^S}{\sin\varphi^S}\left(\cos\varphi_R^S + \cos\varphi_L^S\right).\end{aligned}$$

By using $\Gamma_L = \frac{a}{a+1}\Gamma$ in Eq. (A1), the expression for the current incoming to the left lead for the asymmetric case reads

$$J^A = J_L^A = \frac{2a}{a+1}2k_BT\sum_{\omega_n}\frac{\Gamma\Delta}{\sqrt{\Delta^2+\omega_n^2}}\mathrm{Im}\left[\mathcal{G}(i\omega_n)e^{-i\varphi_L^A}\right]. \tag{A6}$$

Now we do the important step to express J^A in terms of the corresponding J^S. Since the quantities $\mathcal{R},\mathcal{I}$ are invariant under

the transformation (A3), we can insert them into (A6). After simple rearrangement we obtain

$$J^A = -\frac{2a}{a+1}\frac{J^S(\varphi^S)}{\sin\varphi^s}\left\{\sin\left(\varphi_L^S-\varphi_L^A\right)+\sin\left(\varphi_R^S-\varphi_L^A\right)\right\}. \tag{A7}$$

Using the relations (A3) to eliminate $\varphi_{L,R}^S$ yields the gauge invariant form

$$\begin{aligned} J^A(\varphi^A) = &- J^S\frac{2a}{a+1}\frac{1}{\sin(2\arccos\sqrt{\chi})} \\ &\times\left\{\sin\left(\Psi-\frac{\varphi^A}{2}+\arccos\sqrt{\chi}\right)\right. \\ &\left.+\sin\left(\Psi-\frac{\varphi^A}{2}-\arccos\sqrt{\chi}\right)\right\}. \end{aligned} \tag{A8}$$

This is simplified with use of the formula $\sin\alpha+\sin\beta = 2\sin\frac{\alpha+\beta}{2}\cos\frac{\alpha-\beta}{2}$ in the numerator, and $\sin 2\alpha = 2\sin\alpha\cos\alpha$, $\sin\arccos\alpha = \sqrt{1-\alpha^2}$ in the denominator.

$$\begin{aligned} J^A(\varphi^A) &= -J^S\frac{2a}{a+1}\frac{\sin\left(\Psi-\frac{\varphi^A}{2}\right)}{\sin(\arccos\sqrt{\chi})} \\ &= -J^S\frac{2a}{a+1}\frac{\sin\Psi\cos\frac{\varphi^A}{2}-\sin\frac{\varphi^A}{2}\cos\Psi}{\sqrt{1-\chi}}. \end{aligned} \tag{A9}$$

Next, to get rid of Ψ, we compute

$$\begin{aligned} \cos\Psi &= \frac{1}{\sqrt{1+\left(\frac{a-1}{a+1}\right)^2\tan^2\frac{\varphi^A}{2}}} = \frac{\cos\frac{\varphi^A}{2}}{\sqrt{\chi}}, \\ \sin\Psi &= \frac{\left(\frac{a-1}{a+1}\right)\tan\frac{\varphi^A}{2}}{\sqrt{1+\left(\frac{a-1}{a+1}\right)^2\tan^2\frac{\varphi^A}{2}}} = \frac{\left(\frac{a-1}{a+1}\right)\sin\frac{\varphi^A}{2}}{\sqrt{\chi}}. \end{aligned} \tag{A10}$$

After inserting these relations, Eq. (A9) becomes

$$J_L^A = \frac{-\frac{2a}{a+1}\left(\frac{a-1}{a+1}-1\right)\sin\frac{\varphi^A}{2}\cos\frac{\varphi^A}{2}}{\sqrt{\chi}\sqrt{1-\chi}}J^S. \tag{A11}$$

Since the numerator yields $(\chi-1)\cot\frac{\varphi^A}{2}$ (for $\varphi^A\neq 0$), the relation between the Josephson current in the symmetric and asymmetric case is simplified to

$$J^A(\varphi^A) = \sqrt{\frac{(1-\chi)}{\chi}}\cot\frac{\varphi^A}{2}J^S(2\arccos\sqrt{\chi}), \tag{A12}$$

or, explicitly in φ

$$\begin{aligned} J^A(\varphi) = &\frac{\cos\frac{\varphi}{2}}{\sqrt{\frac{(a+1)^2}{4a}-\sin^2\frac{\varphi}{2}}} \\ &\times J^S\left(2\arccos\sqrt{1-\frac{4a}{(a+1)^2}\sin^2\frac{\varphi}{2}}\right), \end{aligned} \tag{A13}$$

which is Eq. (7).

APPENDIX B: LINEARIZATION AND ALTERNATIVE FITTING PROCEDURE

In this Appendix B we present an alternative analysis of the experiment based on linear approximation, which was motivated by the successful use of Eq. (9) by Delagrange *et al.* [25] in most of the measured cases (diamonds B, G, and I). We show that, even though the parabolic fit discussed in the main text is more general, the simpler linear approximation may give good enough results. Moreover, the linear approximation might be relevant in the fully developed Kondo regime.

Applying Eq. (5b) to the phase boundary clearly shows that $\varphi_C(\epsilon)$ has an exactly arc-cosine shape assumed in Eq. (9) if and only if $\chi_C(\epsilon)$ is linear in ϵ. Indeed, from NRG data we observe that for big enough U/Γ the phase boundary approaches a straight line, see Figs. 1(c) and 4. Moreover, when asymmetry is involved, only the values of χ_C close to 1 [blue area in Fig. 1(c)] are used. This means that for large asymmetry the linear approximation becomes relevant for a wider range of parameters.

We therefore assume $\chi_C(\tilde{\epsilon})\approx\kappa-\tilde{\epsilon}/\beta$. Inserting it into Eq. (5b) gives [cf. Eq. (11)]

$$\varphi_C = \arccos\left[-\frac{(a+1)^2}{2a}\left(\frac{\tilde{\epsilon}}{\beta}+\frac{a^2+1}{(a+1)^2}-\kappa\right)\right]. \tag{B1}$$

Comparison with Eq. (9) leads to

$$\widetilde{\delta\epsilon} = \frac{4a}{(a+1)^2}\beta(\epsilon,U,\Gamma,\Delta), \tag{B2}$$

where we have explicitly stated the dependence of the slope β on given model parameters. For the ideal case of a perfectly linear dependence [or large enough U, see Fig. 1(c)], Eq. (B2) separates the asymmetry dependence of the transition width from a universal (i.e., asymmetry-independent) slope β (which also equals the transition width in the symmetric case). For experimentally relevant intermediate U's (red curve in Fig. 1) the curve slightly bends and linear regression restricted to the appropriate range of χ_C is more precise and is used in the next paragraphs to analyze the experimental data.

We have applied Eq. (B2) to find the asymmetry of diamonds B, G, and I from the measured transition width $\widetilde{\delta\epsilon}_{\rm exp}$ and the theoretical slope $\beta_{\rm NRG}$ obtained by performing a linear fit of phase-boundary curves $\chi_C(\tilde{\epsilon})$ calculated via NRG. To account

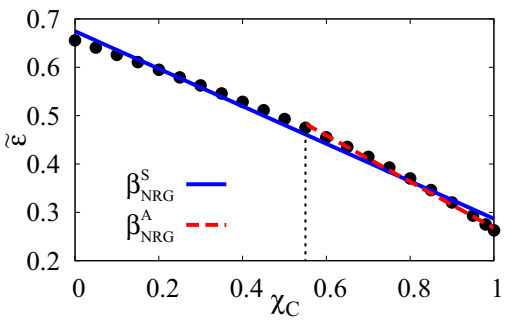

FIG. 5. Illustration of the fitting procedure used to obtain the asymmetry. The numerically determined $\tilde{\epsilon}(\chi_C)$ dependence (bullets) is approximated by a linear fit in the symmetric (blue solid line) and asymmetric (red dashed line) case. The negative slopes are denoted $\beta^S_{\rm NRG}$ and $\beta^A_{\rm NRG}$, respectively. The fitting range for the asymmetric case is marked by the vertical dotted line. In case of perfect linearity the lines would merge, but for a realistic curve on the verge of the Kondo regime they differ slightly.

for their weak nonlinearities, we restrict the fitting range of χ_C only to values $[(a-1)^2/(a+1)^2, 1]$ relevant for the asymmetric case (blue area in Fig. 1). The range (influencing the slope β_{NRG}) and the asymmetry a were determined self-consistently as values matching most closely the experimentally measured transition widths. Figure 5 features the $\tilde{\epsilon}(\chi_C)$ dependence (bullets) calculated by NRG for the diamond B in the experiment of Delagrange *et al.* [25]. We have chosen the diamond B as an illustration, because in this case the linear approximation used to determine the asymmetry is the least accurate [see Fig. 4(c)].

We performed two linear fits. The negative slope denoted as β^A_{NRG} (red dashed line) was obtained using the restricted interval (marked by the vertical dashed line) as discussed in the main text. For comparison, we also include the fit in the whole range $[0,1]$ of χ_C with the negative slope denoted β^S_{NRG} (blue solid line). For a realistic phase-boundary curve the two slopes are close but not completely identical. The values of the β^A_{NRG} used to determine the asymmetry are tabulated in Table I in the main text, while corresponding values of β^S_{NRG} for diamonds B, G, and I, respectively, are 0.388, 0.190, and 0.291. These values are equal to the transition width of a symmetric ($a = 1$) junction. The estimated standard error of the fit of all slopes was less than 2%. Results for the asymmetry are also included in Table I in the main text and are in good agreement with values obtained by the quadratic approximation.

[1] S. De Franceschi, L. Kouwenhoven, C. Schönenberger, and W. Wernsdorfer, Nat. Nano **5**, 703 (2010).

[2] A. Martín-Rodero and A. Levy Yeyati, Adv. Phys. **60**, 899 (2011).

[3] A. F. Morpurgo, J. Kong, C. M. Marcus, and H. Dai, Science **286**, 263 (1999).

[4] A. Y. Kasumov, R. Deblock, M. Kociak, B. Reulet, H. Bouchiat, I. I. Khodos, Y. B. Gorbatov, V. T. Volkov, C. Journet, and M. Burghard, Science **284**, 1508 (1999).

[5] A. Kasumov, M. Kociak, M. Ferrier, R. Deblock, S. Guéron, B. Reulet, I. Khodos, O. Stéphan, and H. Bouchiat, Phys. Rev. B **68**, 214521 (2003).

[6] P. Jarillo-Herrero, J. A. van Dam, and L. P. Kouwenhoven, Nature (London) **439**, 953 (2006).

[7] J. A. van Dam, Y. V. Nazarov, E. P. A. M. Bakkers, S. De Franceschi, and L. P. Kouwenhoven, Nature (London) **442**, 667 (2006).

[8] H. I. Jørgensen, K. Grove-Rasmussen, T. Novotný, K. Flensberg, and P. E. Lindelof, Phys. Rev. Lett. **96**, 207003 (2006).

[9] J. P. Cleuziou, W. Wernsdorfer, V. Bouchiat, T. Ondarcuhu, and M. Monthioux, Nat. Nano **1**, 53 (2006).

[10] H. I. Jørgensen, T. Novotný, K. Grove-Rasmussen, K. Flensberg, and P. E. Lindelof, Nano Lett. **7**, 2441 (2007).

[11] K. Grove-Rasmussen, H. I. Jørgensen, and P. E. Lindelof, New J. Phys. **9**, 124 (2007).

[12] E. Pallecchi, M. Gaass, D. A. Ryndyk, and C. Strunk, Appl. Phys. Lett. **93**, 072501 (2008).

[13] Y. Zhang, G. Liu, and C. Lau, Nano Res. **1**, 145 (2008).

[14] H. I. Jørgensen, K. Grove-Rasmussen, K. Flensberg, and P. E. Lindelof, Phys. Rev. B **79**, 155441 (2009).

[15] G. Liu, Y. Zhang, and C. N. Lau, Phys. Rev. Lett. **102**, 016803 (2009).

[16] A. Eichler, R. Deblock, M. Weiss, C. Karrasch, V. Meden, C. Schönenberger, and H. Bouchiat, Phys. Rev. B **79**, 161407 (2009).

[17] C. B. Winkelmann, N. Roch, W. Wernsdorfer, V. Bouchiat, and F. Balestro, Nat. Phys. **5**, 876 (2009).

[18] J.-D. Pillet, C. H. L. Quay, P. Morfin, C. Bena, A. L. Yeyati, and P. Joyez, Nat. Phys. **6**, 965 (2010).

[19] G. Katsaros, P. Spathis, M. Stoffel, F. Fournel, M. Mongillo, V. Bouchiat, F. Lefloch, A. Rastelli, O. Schmidt, and S. De Franceschi, Nat. Nano **5**, 458 (2010).

[20] R. Maurand, T. Meng, E. Bonet, S. Florens, L. Marty, and W. Wernsdorfer, Phys. Rev. X **2**, 011009 (2012).

[21] E. J. H. Lee, X. Jiang, R. Aguado, G. Katsaros, C. M. Lieber, and S. De Franceschi, Phys. Rev. Lett. **109**, 186802 (2012).

[22] J. D. Pillet, P. Joyez, R. Žitko, and M. F. Goffman, Phys. Rev. B **88**, 045101 (2013).

[23] A. Kumar, M. Gaim, D. Steininger, A. L. Yeyati, A. Martín-Rodero, A. K. Hüttel, and C. Strunk, Phys. Rev. B **89**, 075428 (2014).

[24] R. Delagrange, D. J. Luitz, R. Weil, A. Kasumov, V. Meden, H. Bouchiat, and R. Deblock, Phys. Rev. B **91**, 241401(R) (2015).

[25] R. Delagrange, R. Weil, A. Kasumov, M. Ferrier, H. Bouchiat, and R. Deblock, Phys. Rev. B **93**, 195437 (2016).

[26] S. Li, N. Kang, P. Caroff, and H. Q. Xu, Phys. Rev. B **95**, 014515 (2017).

[27] D. J. Luitz, F. F. Assaad, T. Novotný, C. Karrasch, and V. Meden, Phys. Rev. Lett. **108**, 227001 (2012).

[28] W. Chang, V. E. Manucharyan, T. S. Jespersen, J. Nygård, and C. M. Marcus, Phys. Rev. Lett. **110**, 217005 (2013).

[29] T. Matsuura, Prog. Theor. Phys. **57**, 1823 (1977).

[30] L. I. Glazman and K. A. Matveev, Pis'ma Zh. Eksp. Teor. Fiz. **49**, 570 (1989) [JETP Lett. **49**, 659 (1989)].

[31] A. V. Rozhkov and D. P. Arovas, Phys. Rev. Lett. **82**, 2788 (1999).

[32] T. Yoshioka and Y. Ohashi, J. Phys. Soc. Jpn. **69**, 1812 (2000).

[33] F. Siano and R. Egger, Phys. Rev. Lett. **93**, 047002 (2004).

[34] M.-S. Choi, M. Lee, K. Kang, and W. Belzig, Phys. Rev. B **70**, 020502 (2004).

[35] G. Sellier, T. Kopp, J. Kroha, and Y. S. Barash, Phys. Rev. B **72**, 174502 (2005).

[36] T. Novotný, A. Rossini, and K. Flensberg, Phys. Rev. B **72**, 224502 (2005).

[37] C. Karrasch, A. Oguri, and V. Meden, Phys. Rev. B **77**, 024517 (2008).

[38] T. Meng, S. Florens, and P. Simon, Phys. Rev. B **79**, 224521 (2009).

[39] M. Governale, M. G. Pala, and J. König, Phys. Rev. B **77**, 134513 (2008); D. Futterer, J. Swiebodzinski, M. Governale, and J. König, *ibid.* **87**, 014509 (2013).

[40] A. Oguri, Y. Tanaka, and J. Bauer, Phys. Rev. B **87**, 075432 (2013).

[41] G. Kiršanskas, M. Goldstein, K. Flensberg, L. I. Glazman, and J. Paaske, Phys. Rev. B **92**, 235422 (2015).

[42] T. Domański, M. Žonda, V. Pokorný, G. Górski, V. Janiš, and T. Novotný, Phys. Rev. B **95**, 045104 (2017).

[43] G. D. Mahan, *Many-particle physics* (Plenum, New York, 2000).

[44] M. Žonda, V. Pokorný, V. Janiš, and T. Novotný, Sci. Rep. **5**, 8821 (2015).

[45] M. Žonda, V. Pokorný, V. Janiš, and T. Novotný, Phys. Rev. B **93**, 024523 (2016).

[46] R. Žitko, NRG Ljubljana - open source numerical renormalization group code (2014), http://nrgljubljana.ijs.si; R. Žitko and T. Pruschke, Phys. Rev. B **79**, 085106 (2009).

[47] C. Buizert, A. Oiwa, K. Shibata, K. Hirakawa, and S. Tarucha, Phys. Rev. Lett. **99**, 136806 (2007).

[48] With T_K from our Eq. (8) which differs from T_K used in Ref. [32] by a multiplicative factor $\approx$0.41 and correspondingly changes the phase-boundary condition.

[49] We used a nonlinear least-squares procedure within `Gnuplot`; for the description of statistical errors see the documentation page http://gnuplot.sourceforge.net/docs_4.2/node86.html.

[50] One point can be chosen with $\varphi_C = 0$ which is equivalent to a QD coupled to a *single* superconducting lead and amounts to a single-channel NRG problem that can be handled rather easily. The second point will necessarily involve a two-channel NRG problem which is more computationally demanding. Still the computational requirements boil down basically to a single set of two-channel NRG calculations to determine one phase-boundary point, which is very moderate.